



# Global high-resolution forest disturbance type dataset

Li Wang<sup>1</sup>, Shidong Liu<sup>1\*</sup>, Wanjuan Song<sup>1</sup>, Jie Zhang<sup>2, 3</sup>, Shengping Ding<sup>4</sup>

<sup>1</sup>State Key Laboratory of Remote Sensing and Digital Earth, Aerospace Information Research Institute, Chinese Academy of Sciences, Beijing 100094, China;

5 <sup>2</sup>School of Land Science and Technology, China University of Geosciences (Beijing), Beijing 100083, China;

<sup>3</sup>Department of Earth System Science, Ministry of Education Key Laboratory for Earth System Modeling, Institute for Global Change Studies, Tsinghua University, Beijing 100084, China;

<sup>4</sup>Faculty of Science, University of Copenhagen. Copenhagen 1350, Denmark

*Correspondence to:* Shidong Liu (liusd@aircas.ac.cn)

10 **Abstract.** Forests play a pivotal role in global carbon cycling and biodiversity conservation, yet they face increasing  
disturbances from both anthropogenic and natural drivers. This study presents the first high-resolution (30-m) global forest  
disturbance dataset (GFD) for 2000–2020, classifying 11 disturbance types by integrating Landsat-based Continuous Change  
Detection and Classification (CCDC) time-series analysis with spatial metrics and machine learning. A total of 57,000  
expert-validated samples were used to train and validate a decision tree model, achieving an overall accuracy of 94.88%. The  
15 results reveal that forestry disturbance (43.79±0.31%), shifting cultivation (24.32±0.28%), and forest fires (11.45±0.05%)  
dominate global forest loss. There are regional differences in global forest disturbance, such as farmland expansion in South  
America and Africa, forest fires in northern regions, and shifting cultivation in tropical regions. Disturbed forests span  
1,247.06±11.18Mha, accounting for 30.87% of the global forest area. Notably, 2.76% of global forests were newly  
established, primarily in China, India, and Brazil. Spatial consistency analysis with existing datasets ( $R^2=0.93$ ) confirms the  
20 reliability of the GFD product. The GFD dataset advances our understanding of forest dynamics and underscores the need  
for targeted conservation strategies in an era of escalating environmental change. The 30 m resolution GFD generated by this  
study is openly available at <https://doi.org/10.6084/m9.figshare.28465178> (Liu et al., 2025a).

## 1 Introduction

25 Forests, the dominant component of terrestrial ecosystems and the most widespread vegetation type on land, play a  
pivotal role in delivering critical ecosystem services, including climate regulation (Piao et al., 2020; Xu et al., 2022),  
biodiversity conservation (Betts et al., 2017), soil and water retention, carbon sequestration (Tong et al., 2020), and habitat  
provision (Oeser et al., 2021). However, in recent decades, forest ecosystems have faced escalating disturbances from both  
natural drivers (Leverkus et al., 2018; Yan et al., 2022; Mayer et al., 2024) (droughts, extreme rainfall, and wildfires  
exacerbated by climate anomalies) and anthropogenic activities (deforestation, shifting cultivation, cropland expansion, and  
30 urbanization) (Acil et al., 2025; Chowdhury et al., 2017; Rivera et al., 2023; Liu et al., 2025b). These disturbances have  
severely compromised forest composition, structure, and functionality, thereby degrading their ecological services (Yang et



al., 2020; Feng et al., 2021). Consequently, accurate, timely, and continuous monitoring of forest disturbances is imperative for effective forest management, climate change mitigation, and global carbon accounting.

Forest disturbance represents one of the most critical processes in ecosystem succession (Ross et al., 2021; Mason et al., 2019; Blaschke et al., 1992), essential for maintaining regional ecological equilibrium (Reza and Abdullah, 2011; Kittel et al., 2000). Forest dynamics encompass two opposing processes: disturbance (forest cover loss or structural degradation caused by natural or human factors) and gain (forest recovery through natural regeneration or afforestation). Rapid population growth and urbanization have intensified conflicts between natural resource exploitation and human activities (Jiang et al., 2021; Miatto et al., 2021). Thus, characterizing the spatiotemporal patterns of forest disturbance and gain is vital for understanding forest dynamics, estimating carbon stocks, and elucidating global change mechanisms (Chen et al., 2023b; Cuni-Sanchez et al., 2021; Peng et al., 2023). Given this context, high-accuracy identification of disturbance types has emerged as a key scientific challenge in global environmental governance and sustainable development.

Traditional forest monitoring predominantly relies on field surveys, which suffer from subjectivity, low temporal resolution, and high labor costs, rendering them inadequate for large-scale applications (Scheeres et al., 2023; Finger et al., 2021). Satellite remote sensing has revolutionized this field by offering extensive spatial coverage, continuous temporal observations, and rich spectral information (Zhao et al., 2023; Skidmore et al., 2021). Early remote sensing approaches, such as bi-temporal image comparison (post-classification change detection or spectral differencing), were limited by their sensitivity to image registration accuracy and inability to capture gradual disturbances (Wang et al., 2021). Pixel-based methods (NDVI thresholding) could detect vegetation changes but failed to discriminate disturbance types (deforestation, fires, or shifting cultivation).

Recent advances in time-series analysis have significantly improved monitoring capabilities (Tollerud et al., 2023; Liu et al., 2024). For instance, the Continuous Change Detection and Classification (CCDC) algorithm decomposes Landsat time-series data into trend, seasonal, and noise components, enabling disturbance detection at 30-m resolution (Tollerud et al., 2023; Hwang et al., 2022). Nevertheless, these methods exhibit notable limitations: inadequate spectral-temporal feature integration, leading to high confusion errors between plantation rotation and shifting cultivation; and poor model generalizability, algorithms like CUSUM, developed for temperate forests, underperform in tropical regions due to cloud contamination and phenological variability (Aquino et al., 2022; Ygorra et al., 2021).

To address these challenges, we propose a machine learning framework that synergizes time-series features with spatial aggregation metrics, leveraging the nonlinear modeling strengths of ensemble algorithms. This study aims to produce the first high-resolution (30-m) global map of 11 major forest disturbance types (Table 1) in 2000–2020 by integrating Landsat CCDC time-series and spatial predictors within Google Earth Engine (GEE). To account for regional heterogeneity in forest types, climate regimes, and disturbance drivers, we partitioned the globe into four subregions for model training. Our results will directly support the Paris Agreement’s carbon accounting framework, provide subtype data for platforms like Global Forest Watch (GFW) and Hansen’s global forest change dataset, and inform regional forest restoration strategies.

**Table 1: Global forest disturbance classification framework**



Code	Disturbance type	Disturbance intensity	Disturbance source	Forest type	Disturbance process	Recovery type
0	Undisturbed	Undisturbed	-	Natural forests	Undisturbed between 2000 and 2020.	-
11	Shifting cultivation	Strong	Human disturbance	Natural forests	Residents randomly cut down forests on a small scale and plant crops, then abandon cultivation after 1-2 years.	Natural recovery
12	Forestry disturbance	Strong	Human disturbance	Natural forests	To obtain wood, natural forests were cut down, and later manual planted them.	Manual reversion
13	Plantation disturbance	Strong	Human disturbance	Plantation	Regular logging and renewal of plantations.	Manual reversion
14	Deforestation of natural forests	Strong	Human disturbance	Natural forests	To obtain wood, natural forests were cut down, and later natural recovery.	Natural recovery
15	Forest fire disturbance	Strong	Natural fire	All forests	The destruction of forests by wildfires.	Natural recovery
16 *	Drought	Weak	Natural climate	All forests	Forest degradation caused by drought.	-
17 *	Forest pests and diseases	Weak	Natural pests and diseases	All forests	Forest degradation caused by pests and diseases.	-
18	Built-up area expansion	Strong	Human disturbance	All forests	Expansion of built-up areas encroach on forests.	No recovery
19	Cropland occupation	Strong	Human disturbance	All forests	Expansion of cropland encroach on forests.	No recovery
20	Flood disaster	Strong	Natural flood	All forests	Flood disasters encroach on forests.	Natural recovery
21	Oil palm	Strong	Human disturbance	All forests	Expansion of oil palm plantations encroach on forests	Manual reversion
22	Newly added forest	Negative	Human disturbance	Non forest	Artificially planting forests on non-forest land.	Manual planting

Note: \* indicates weak disturbance type. Due to the spatial overlap between weak and strong disturbance types, this study did not consider weak disturbances.

## 2. Materials and methods

### 2.1 Study workflow

70 We developed a novel classification algorithm using machine learning within the GEE platform that integrates Landsat-based CCDC time-series analysis with spatial characteristics of forest cover to classify main distinct forest disturbance types globally. The model training and validation incorporated 57,000 expertly labeled samples of forest disturbance, which were visually interpreted by trained remote sensing specialists specializing in forest monitoring. Utilizing multi-temporal Landsat data in 2000-2020 and ancillary datasets (Section 2.2.5), we constructed a comprehensive feature set comprising 18  
 75 disturbance indicators (Table 2). These features were systematically derived from both temporal and spatial dimensions, including: Overall characteristics of forest disturbance (OC), pre-disturbance forest conditions (PDC), post-disturbance recovery patterns (PDP), disturbance potential metrics (DP), land use/cover features (LUC), spatial contextual attributes (SC). All feature variables were preprocessed in GEE and subsequently resampled to correspond with the 57,000 samples. The classifier was locally trained using Python3.9, with rigorous validation performed at sample locations. Our classification  
 80 approach employed a decision tree-based machine learning algorithm (CRAT), with accuracy metrics quantitatively assessed using independent test samples (Fig. 1).



**Table 2 Global Forest Disturbance Characteristics Indicator**

Indicator type	Forest disturbance characteristic indicators		
OC	Disturbance frequency	Average disturbance period	Number of segments
PDC	Linear intercept before disturbance	Internal fluctuations before disturbance	Interannual trend before disturbance
PDP	Linear intercept after disturbance	Internal fluctuations after disturbance	Interannual trend after disturbance
DP	Forest fire area	Plantation area	Intensity of population
LUC	2020 Land Use /Cover	Forest cover in 2000	Forest cover in 2020
SC	Longitude	Latitude	Disturbance partition

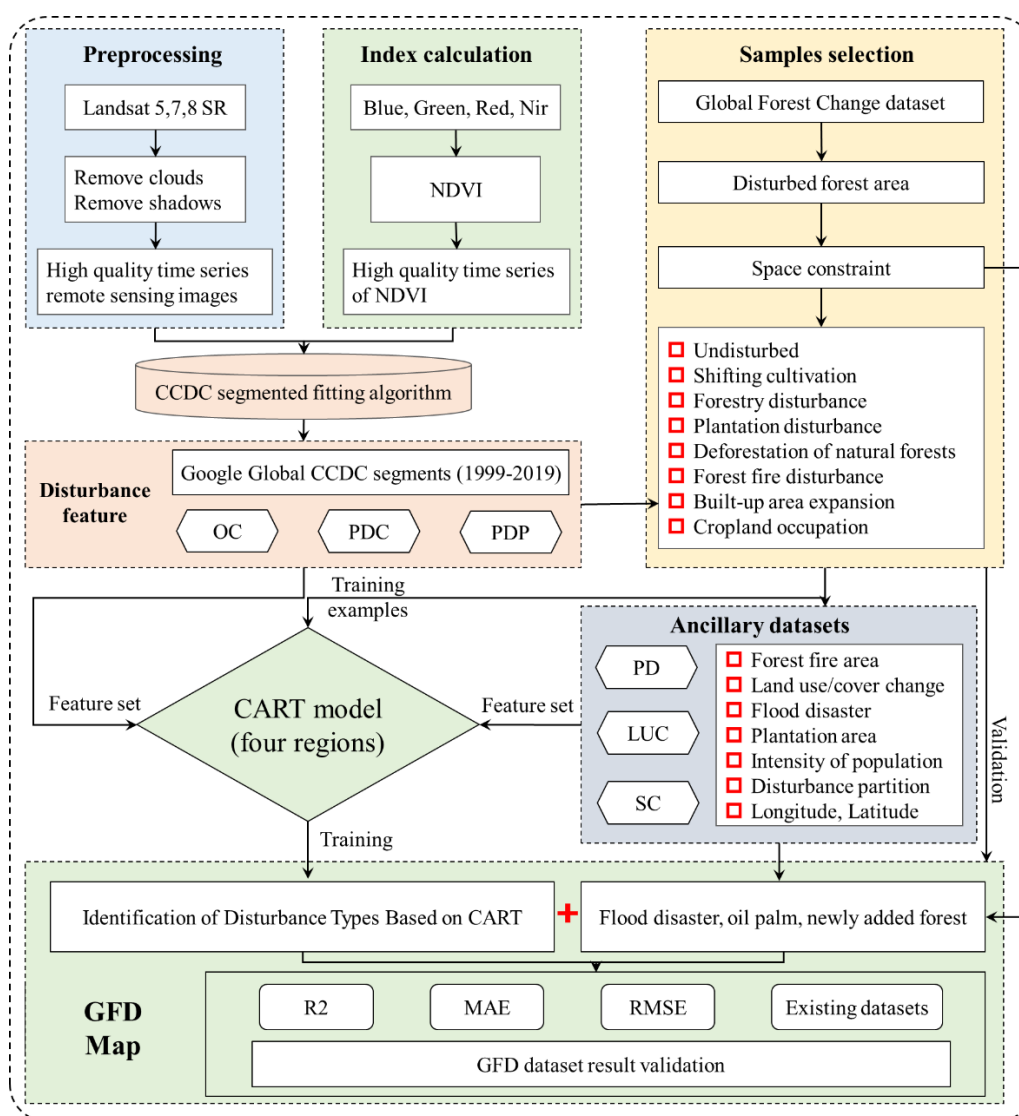


**Figure 1 Study workflow**



## 2.2 Data collection and preprocessing

### 2.2.1 Landsat Image

The first layer surface reflectance (SR) image of Landsat Collection 1 (C1) is selected, including all available Landsat 5-8 images from 2000 to 2020. These images, which have undergone atmospheric correction using the LaSRC algorithm (Skakun et al., 2021), were directly obtained from the GEE platform (<https://developers.google.com/earth-engine/datasets/catalog/landsat> Last visit date: May 10, 2025). We preprocessed global images based on the quality assessment (QA) bands of Landsat SR, including removing shadows and cloud interference. These data are used to calculate CCDC to supplement the current missing CCDC dataset in some forest disturbance areas. At the same time, high-quality Landsat images are also the main dataset for us to visually select samples.

### 95 2.2.2 Spatial distribution dataset

Previous studies have shown that global forest disturbances have a high degree of spatial clustering (Hansen et al., 2013). For example, shifting cultivation is mainly distributed in the tropics (Chen et al., 2023a); Forest fires are mainly distributed in northern forests (Scholten et al., 2021). Adding spatial distribution information of forests is beneficial for improving the accuracy of forest disturbance identification. Considering the regional differences in the distribution of global forest disturbances, we have also divided the global forest disturbance atmosphere into four major clusters: Africa, Southeast Asia Australia, Central America South America, and the Northern Forest Region. Therefore, we added latitude and longitude information as well as partition information when extracting the spatial attributes of the samples. A large number of non-forest areas and undisturbed regions around the world do not require calculation. In order to reduce the consumption of computing power, we use Hansen's global forest change dataset to identify disturbed forest areas worldwide from 2000 to 105 2020 (Hansen et al., 2013).

### 2.2.3 Land use/cover dataset

To assess the mapping accuracy of global forest change areas, this study incorporated multiple authoritative land cover and forest cover products as reference datasets, including: (1) ESA WorldCover 2020, (2) Global Forest Change dataset (Hansen et al., 2013), and (3) the Global Forest Cover Change dataset (Roffe et al., 2022). These datasets served three 110 primary functions in our analysis: delineating the global forest extent in 2000, identifying 2020 forest cover distribution, and classifying non-forest land cover types in 2020. The detailed information of these datasets is systematically documented in Table 3.

**Table 3: Source of Land Cover Dataset**

Dataset	Resolution	Dataset source and main purpose
ESA WorldCover 2020	10m	Used to assist in identifying disturbances in cropland, built-up areas, etc. <a href="https://worldcover2020.esa.int/">https://worldcover2020.esa.int/</a>



---

Global Forest Change dataset	30m	Used to assist in identifying disturbed areas. <a href="https://www.globalforestwatch.org/map/">https://www.globalforestwatch.org/map/</a>
Global Forest Cover Change dataset	30m	Used to assist in identifying disturbed areas. <a href="https://lpdaac.usgs.gov/products/gfcc30tecv003/">https://lpdaac.usgs.gov/products/gfcc30tecv003/</a>

---

#### 115 2.2.4 Disturbance feature

The CCDC algorithm is commonly used to monitor surface cover disturbances (Zhu and Woodcock, 2014). It fits the model to the Normalized Difference Vegetation Index (NDVI) of spectral observations and can reflect three types of pixel changes: seasonal changes (such as phenology), slow changes (such as vegetation growth or degradation), and rapid changes (such as deforestation, fires) (Zhu and Woodcock, 2014). CCDC uses a powerful iterative reweighted least squares method (RIRLS) (Burrus et al., 1994) to fit the observed geomorphological features and trends that reflect phenology (Tollerud et al., 2023; Hwang et al., 2022). The expression for the mathematical fitting line is as follows:

$$\widehat{NDVI}(x)_{RIRLS} = a_0 + a_1 \cos\left(\frac{2\pi}{T}x\right) + b_1 \sin\left(\frac{2\pi}{T}x\right) + a_2 \cos\left(\frac{2\pi}{NT}x\right) + b_2 \sin\left(\frac{2\pi}{NT}x\right) \quad (1)$$

Where  $x$  represents day of year;  $T$  represents the number of days per year;  $N$  represents the number of years of Landsat.  $a_0$  represents the benchmark value of NDVI;  $a_1$  and  $b_1$  represent the annual changes in NDVI;  $a_2$  and  $b_2$  represent the interannual changes in NDVI.  $\widehat{NDVI}(x)_{RIRLS}$  represents the predicted value of NDVI based on RIRLS fitting corresponding to the  $x$ -th day of year.

We collected Google Global Landsat based CCDC segments (1999-2019). The dataset was created from the Landsat 5, 7, and 8 Collection-1, Tier-1, surface reflectance time series, using all daytime images between 1999-01-01 and 2019-12-31. Each image was preprocessed to mask pixels identified as cloud, shadow, or snow (according to the 'pixel\_qa' band), saturated pixels, and pixels with an atmospheric opacity > 300 (as identified by the 'sr\_atmos\_opacity' and 'sr\_aerosol' bands). Pixels repeated in north/south scene overlap were deduplicated. The results were output in 2-degree tiles for all landmasses between -60° and +85° latitude. We can directly call this dataset [ee.ImageCollection("GOOGLE/GLOBAL\_CCDC/V1")] in GEE. For the vacant areas in the dataset, the CCDC algorithm is used to complete them, thereby obtaining vegetation change characteristics covering all forest areas worldwide. Based on the segmented fitting results of these features, we extracted the OC, PDC, and PDP of each pixel separately (Fig. 2).

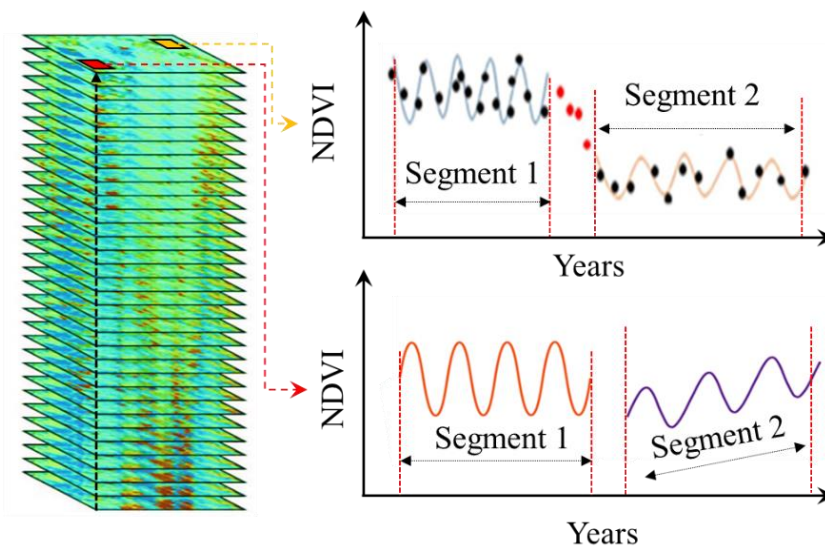


Figure 2 CCDC fitting process.

### 2.2.5 Ancillary datasets

Forest disturbance has strong disturbance sources. Therefore, using existing disturbance source datasets to assist in  
140 identifying typical forest disturbance types can effectively improve the accuracy of mapping results. Considering the high  
consistency between disturbance types such as forest fires and plantation expansion and global fire and plantation  
distribution. This study uses global fire distribution datasets, artificial plantation distribution datasets, oil palm datasets, and  
other auxiliary methods to identify forest disturbance types. Meanwhile, there is a high correlation between population  
distribution and forest disturbance. This study collected a forest disturbance potential dataset from three aspects: population  
145 density, forest fire distribution, and spatial distribution of oil palms.

### 2.3 Samples selection

The selection of samples mainly refers to the time series changes of Landsat images from 2000 to 2020 and the  
historical images of high-resolution Google images. Based on literature and actual disturbance image characteristics, 8 types  
of forest disturbances have been preliminarily identified through research: undisturbed (0), shifting cultivation disturbance  
150 (11), forestry disturbance (12), plantation disturbance (13), deforestation of natural forests (14), forest fire disturbance (15),  
built-up area expansion (18), and cropland occupation (19). For 8 elementary disturbance types, 12 well-trained forest  
remote sensing professionals visually identified 57000 forest disturbance type samples for over 300 hours. To ensure global  
consistency in sample selection, 8 individuals were uniquely responsible for selecting 8 types, while an additional 4  
individuals conducted secondary confirmation of the selected samples. The samples are evenly distributed in the global  
155 forest disturbance area. For the forest weak disturbance types caused by drought disturbance (16) and pest disturbance (17),



their sample selection needs to refer to high-resolution long-term remote sensing images. Meanwhile, due to the high timeliness of weak disturbances in forests. For example, the decline in vegetation index caused by a period of drought will quickly recover due to an increase in precipitation. At the global scale, it is currently limited by the availability of remote sensing images. We are unable to select relevant samples through Landsat imagery. Therefore, this study did not consider these two weak disturbance types of drought disturbance and pest disturbance are not considered.

## 2.4 Decision Tree Classification Model

### 2.4.1 Identification of Disturbance Types Based on CART Method

Considering that the core of this study is forest disturbance type classification, the Classification and Regression Tree (CART) classification regression tree algorithm, which has a high advantage in convenient classification, was chosen. In this article, we only discuss CART used for classification. For classification trees, CART uses the Gini coefficient minimization criterion for feature selection to generate binary trees. The specific process includes the following two steps: Decision tree generation: generate a decision tree based on the training dataset, and the generated decision tree should be as large as possible; Decision tree pruning: Use the validation dataset to prune the generated tree and select the optimal subtree, with the minimum loss function as the criterion for pruning.

Considering the significant differences in disturbances in different regions of the world, four CART sub decision trees were trained for four typical disturbance regions, namely Africa, Southeast Asia Australia, Central America South America, and the Northern Forest region, to form a larger global forest disturbance classification tree model. The entire process is completed interactively on three platforms: Python, GEE, and ArcGIS. 40000 sample points are used for model training, and another 17000 sample points are used to validate the model training results.

### 2.4.2 Identification of other types of forest disturbance

Based on the preliminary identification of 8 types of forest disturbances and the global forest change range by CART, considering the dynamic changes of flood inundation areas from 200 to 2020, the forest areas that have been submerged by floods are determined, and then flood disaster disturbances are classified (20). Meanwhile, based on the distribution of oil palm in the plantation, the interference of oil palm since 2000 has been extracted (21). In addition, by overlaying the forest coverage in 2000 and the quantity coverage in 2020, the newly added forest areas in 2020 were extracted from the non-forest areas in the early stage (22). Finally, this study generated a global forest disturbance type dataset containing 11 forest disturbance types.

## 2.5 Verification of results

We overlay validation samples and generated GFD maps to calculate confusion matrices and evaluate user, producer, and overall accuracy.



### 2.5.1 Error matrix

The error matrix is a simple cross tabulation of class labels assigned by remote sensing data classification and reference data of sample locations. The error matrix organizes the collected sample data in a way that summarizes key results and helps quantify accuracy and area of various types of forest disturbance. The main diagonal of the error matrix highlights the correct classification, while the diagonal elements show omissions and errors. The cell entries and marginal values of the error matrix are the basis for accuracy evaluation and area estimation. In the matrix,  $p_{ij}$  represents the proportion of samples with map class  $i$  and reference class  $j$ .

Overall accuracy ( $OA$ ) derived from the overall error matrix of 11 forest disturbance types:

$$OA = \sum_{j=1}^{11} p_{jj} \quad (2)$$

User's accuracy for Class  $i$  ( $U_i$ ) (the proportion of regions mapped to class  $i$  with reference to class  $i$ )

$$U_i = p_{ii}/p_{i.} \quad (3)$$

Producer's accuracy for class  $j$  (proportion of samples with class  $j$  mapped to reference class  $j$ )

$$P_j = \frac{p_{jj}}{p_{.j}} \quad (4)$$

### 2.5.2 Estimating accuracy

According to the accuracy evaluation methods of existing research (Olofsson et al., 2014), suppose the sample-based estimator of  $p_{ij}$  is denoted as  $\hat{p}_{ij}$ . For equal probability sampling designs and for stratified random sampling in which the strata correspond to the map classes:

$$\hat{p}_{ij} = W_i \frac{n_{ij}}{n_i} \quad (5)$$

where  $W_i$  is the proportion of area mapped as class  $i$ .

The sampling variability associated with the accuracy estimates should be quantified by reporting standard errors. The variance estimators are provided below, and taking the square root of the estimated variance results in the standard error of the estimator. For overall accuracy, the estimated variance is:

$$\hat{v}(\hat{O}) = \sum_{i=1}^{12} \frac{W_i^2 \hat{U}_i (1 - \hat{U}_i)}{n_i - 1} \quad (6)$$

For user's accuracy of map class  $i$ , the estimated variance is

$$\hat{v}(\hat{U}_i) = \frac{\hat{U}_i (1 - \hat{U}_i)}{n_i - 1} \quad (7)$$

For producer's accuracy of reference class  $j = k$ , the estimated variance is



$$\hat{V}(\hat{P}_j) = \frac{1}{\hat{N}_j^2} \left[ \frac{N_j^2 (1 - \hat{P}_j)^2 \hat{U}_j (1 - \hat{U}_j)}{n_i - 1} + \hat{P}_j^2 \sum_{i \neq j}^{12} \frac{N_i^2 \frac{n_{ij}}{n_i} \left(1 - \frac{n_{ij}}{n_i}\right)}{n_i - 1} \right] \quad (8)$$

$$\hat{N}_j = \sum_{i=1}^{12} \frac{N_i}{n_i} n_{ij} \quad (9)$$

Where  $\hat{N}_j$  is the estimated marginal total number of pixels of reference class  $j$ ;  $N_i$  is the marginal total of map class  $i$ ;  
 215  $n_i$  is the total number of sample units in map class  $i$ .

### 2.5.3 Estimation of Area and Uncertainty of Various Forest Disturbance Types

The standard deviation estimation formula for the area of each disturbance type  $j$  is:

$$S(p_j) = \sqrt{\sum_i \frac{w_{i \times p_j} - p_j^2}{n_i - 1}} \quad (10)$$

Where,  $n_i$  is the sample count at cell  $(i, j)$  in the error matrix;  $w_i$  is the area proportion of map class  $i$ . The estimated  
 220 area of class  $j$  is  $\hat{A}_j = A \times \hat{P}_j$ , where  $A$  is the total map area, with a value of 13Gha of the total global land area  
 (<https://data.worldbank.org/indicator/AG.LND.TOTL.K2?end=2022&start=1961&view=chart>). The standard error of the  
 estimated area is given by:

$$UA_j = \pm S(p_j) * A \quad (11)$$

An approximate 95% confidence interval is obtained as  $\hat{A}_j \pm 1.96 * UA_j$ .

### 225 2.5.4 Comparison with existing datasets

We compared existing datasets to calculate the errors of typical forest disturbance types. At the global scale, the  
 currently available dataset, ‘‘Classifying drivers of global forest loss (CDGFL)’’, has a relatively low resolution (10 km)  
 (Curtis et al., 2018), and the concept of forest loss differs from that of forest disturbance in this study. Therefore, the absolute  
 area of forest loss under different drivers cannot be directly compared with the forest area under different disturbance types.  
 230 Consequently, we only compared the proportional characteristics of forest cover under the same drivers and disturbance  
 types across different global regions to validate the accuracy of our global spatial distribution of forest disturbances.

Here, we divided the global continental area into 200 grids ( $n$ ) with spatial location information, each measuring  $10^\circ \times$   
 $10^\circ$ . First, we calculated the proportion of forest loss area under different drivers within each grid relative to the global forest  
 loss area, denoted as  $p_i$ , where  $i$  represents the driver type. Second, we calculated the proportion of forest area under different  
 235 disturbance types within each grid relative to the global forest disturbance area, denoted as  $q_i$ , where  $i$  represents the  
 disturbance type. The accuracy of this study was determined by examining the spatial consistency between these two  
 proportions. The primary metrics used for validation included the coefficient of determination ( $R^2$ ) from linear regression,  
 mean absolute error (MAE), and root mean square error (RMSE).



240

$$R^2 = 1 - \frac{\sum_i^n (q_i - p_i)^2}{\sum_i^n (\bar{q}_i - p_i)^2} \quad (12)$$

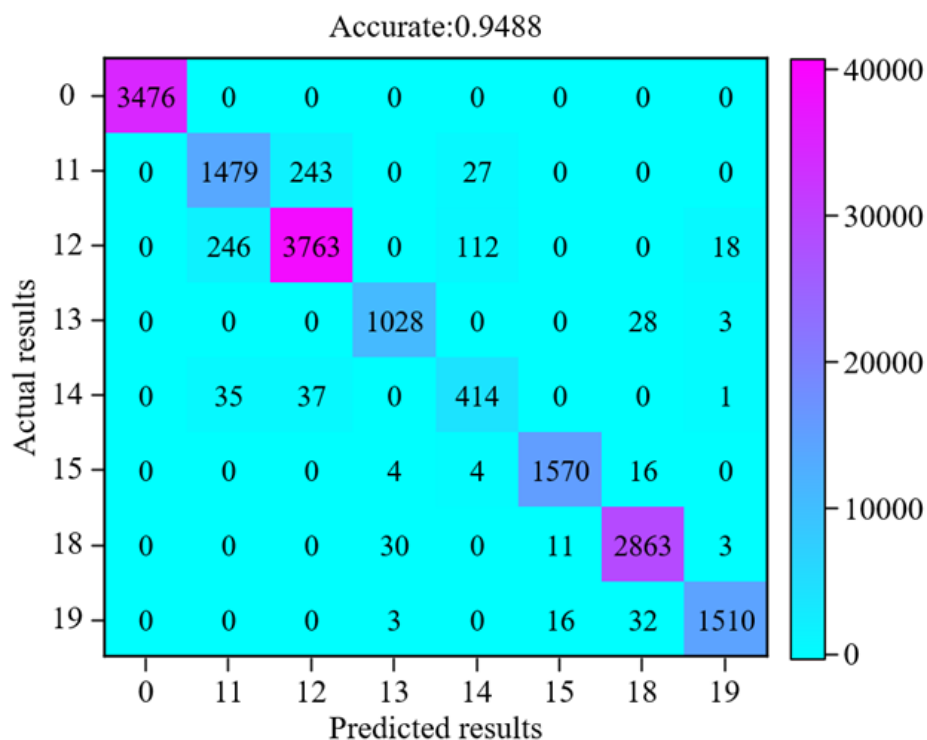
$$MAE = \frac{1}{n} \sum_i^n |p_i - q_i| \quad (13)$$

$$RMSE = \sqrt{\frac{1}{n} \sum_i^n (p_i - q_i)^2} \quad (14)$$

### 3. Result

#### 3.1 Accuracy verification of GFD mapping results

The confusion matrix validation results indicate an overall accuracy of 94.88% (Fig. 3). The highest confusion occurs  
 245 between shifting cultivation and forestry disturbance, as well as deforestation of natural forests, though the accuracy remains relatively high. The identification accuracy for disturbances such as fire reaches nearly 98%. Here, there is no validation of the three disturbance types of oil palm, flood disaster, and newly added forests, as the identification of these disturbance types is based on the superposition with existing datasets, and their accuracy directly depends on the accuracy of the reference dataset.



250

Figure 3 Confusion Matrix of Global Forest Disturbance Classification



The accuracy assessment results reveal significant variations in classification performance across different forest disturbance types. The overall accuracy reaches 94.88% ( $\pm 2.86\%$ ), indicating robust model performance at the aggregate level (Table 4). Forest fire disturbance (98.31% $\pm 3.1\%$  user's accuracy, 98.49% $\pm 6.15\%$  producer's accuracy) and cropland occupation (98.37% $\pm 7.9\%$ , 96.73% $\pm 14.83\%$ ) demonstrate the highest classification reliability. Forestry disturbance shows strong but slightly more variable accuracy (93.07% $\pm 6.8\%$ , 90.92% $\pm 2.51\%$ ), while Shifting cultivation achieves moderate performance (84.03% $\pm 3.5\%$ , 84.56% $\pm 3.96\%$ ). Deforestation of natural forests exhibits the lowest user's accuracy (74.33% $\pm 5.3\%$ ), suggesting significant confusion with other disturbance types, despite its relatively higher producer's accuracy (85.01% $\pm 2.31\%$ ). Built-up area expansion shows nominally high accuracy (97.41% $\pm 9.6\%$ ) but with substantial uncertainty in producer's accuracy ( $\pm 19.66\%$ ). These results highlight both the model's effectiveness for dominant disturbance types.

**Table 4 Accuracy Evaluation of GFD Mapping Results**

Type	User's Accuracy	$\pm$	Producer's Accuracy	$\pm$	Overall Accuracy
11	84.03%	3.5%	84.56%	3.96%	94.88% $\pm$ 2.86%
12	93.07%	6.8%	90.92%	2.51%	
13	96.53%	5.1%	97.07%	3.22%	
14	74.33%	5.3%	85.01%	2.31%	
15	98.31%	3.1%	98.49%	6.15%	
118	97.41%	9.6%	98.49%	19.66%	
19	98.37%	7.9%	96.73%	14.83%	

### 3.2 The spatial distribution of GFD

A high-resolution forest disturbance distribution map of the world has been developed (Fig. 4). The global forest cover disturbance changes mainly occur in South America, Asia, Africa, and North America, accounting for 24.20%, 23.38%, 19.83%, and 18.19% of the total, respectively. The evergreen coniferous forest exhibits significant disturbance in the central Cordillera Mountains, southern Labrador Plateau, Eastern European Plain, and Western Siberian Plain in North America. In the northern part of Eurasia, forest fires remain the most important factor affecting forests. Significant changes in evergreen broad-leaved forests have been observed in the southern Amazon Basin, South Asia, and Indonesia.

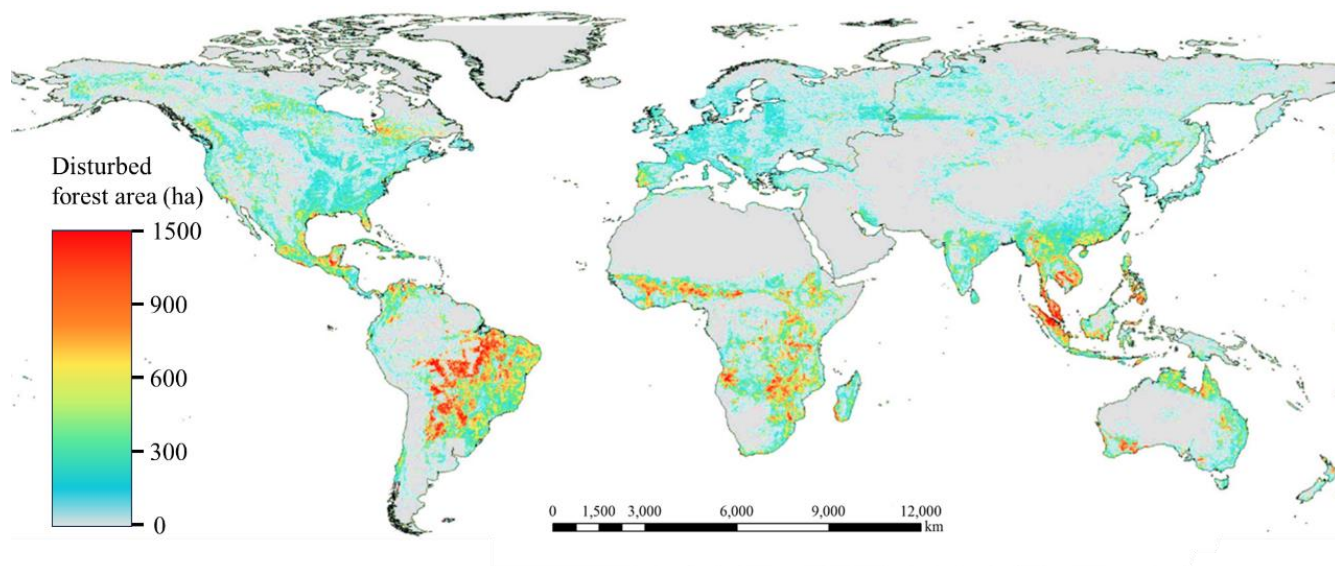


**Figure 4 Global Forest Disturbance Distribution Map**

Between 2000 and 2020, the area of disturbed forests worldwide reached 1247.06 Mha, accounting for 30.87% of the global forest area. The main types of global forest disturbance are forestry disturbance (43.79%), shifting cultivation (24.32%), and forest fires (11.45%) (Fig. 5). The large-scale deforestation of natural forests also accounts for 8.77% of global forest disturbance. The disturbance to forests caused by the cropland occupation, plantation disturbance, oil palm cultivation, and built-up area expansion also accounted for 3.97%, 2.00%, 0.78%, and 0.22%, respectively. Meanwhile, the newly added forests worldwide account for 2.76% of the global forest disturbance area.

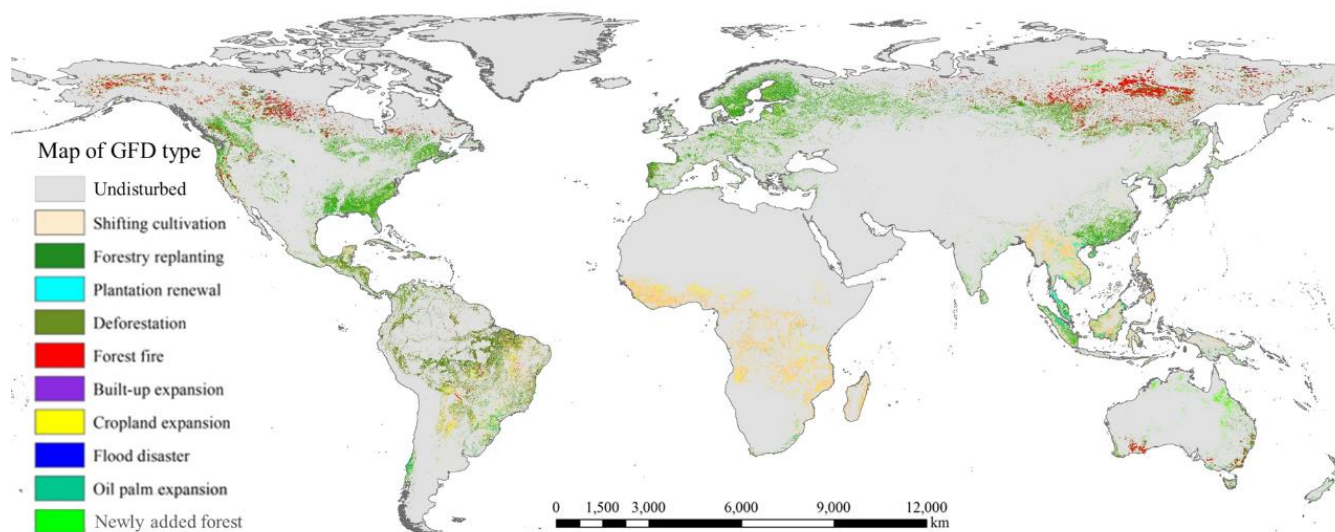


**Figure 5 Global Forest Disturbance Classification Map**



### 3.3 Assessment of disturbance areas and uncertainties

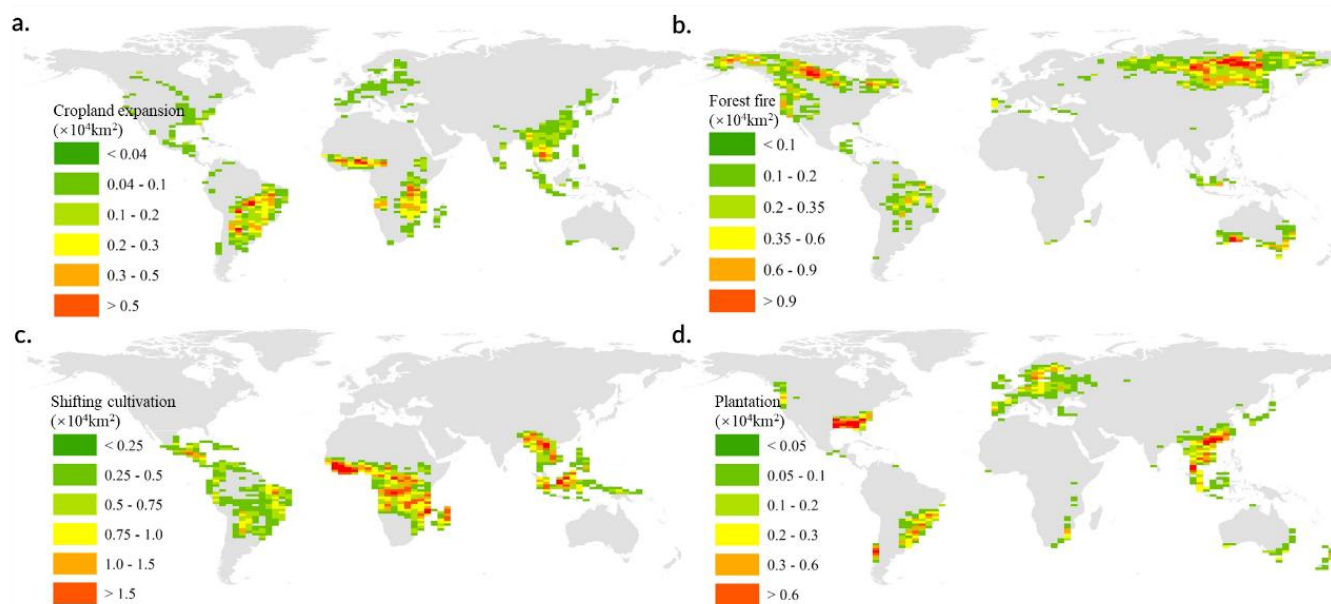
We provide a detailed breakdown of the spatial area and measurement uncertainties for different types of GFD, which represent areas of forest ecosystems affected by anthropogenic or natural disruptions (Table 5). The total disturbed area spans 1247.06±11.8 Mha, with forestry disturbance being the most extensive at 546.03 Mha (43.79% of total GFD), followed by shifting cultivation (303.25 Mha, 24.32%) and forest fire disturbance (142.82 Mha, 11.45%). Together, these three types dominate the dataset, accounting for 80% of all documented forest disturbances. The uncertainty analysis underscores the confidence levels in these estimates. The aggregate uncertainty for the total GFD area is ±0.90% (±11.18 Mha), indicating robust precision at the global scale. However, disparities emerge at the subtype level: forestry disturbance has the highest absolute uncertainty (±3.81 Mha, ±0.31%), reflecting challenges in mapping large, heterogeneous disturbances. In contrast, plantation disturbance exhibits the lowest uncertainty (±0.15 Mha, ±0.01%). For other types, relative uncertainties range from ±0.03% (built-up area expansion) to ±0.19% (deforestation of natural forests), with absolute values between ±0.33 Mha and ±2.41 Mha, respectively. These findings highlight the uneven distribution of forest disturbances and the need for targeted improvements in monitoring systems. The dominance of forestry disturbance, shifting cultivation, and forest fire disturbance suggests they should be prioritized in global forest conservation strategies.

**Table 5: Area and Uncertainty of GFD**

Indicators	Type of GFD									
	11	12	13	14	15	18	19	20	21	22
Area of each type (Mha)	303.25	546.03	24.99	109.37	142.82	2.8	49.46	24.23	9.69	34.44
Area of total GFD (Mha)	1247.06									
% of total GFD	24.32	43.79	2.00	8.77	11.45	0.22	3.97	1.94	0.78	2.76
Uncertainty (±%)	0.28	0.31	0.01	0.19	0.05	0.03	0.03	/	/	/
Total uncertainty (±%)	0.90									
Uncertainty (±Mha)	3.49	3.81	0.15	2.41	0.61	0.33	0.39	/	/	/
Total uncertainty (±Mha)	11.18									

### 3.4 Spatial distribution of typical GFD

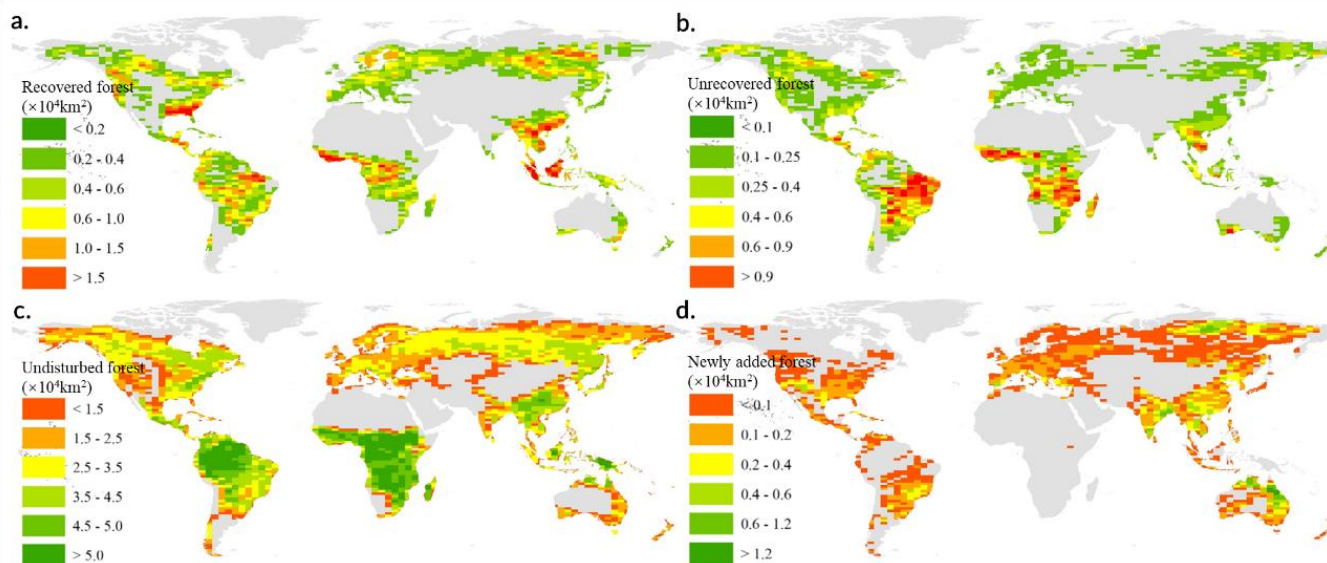
The encroachment of cropland expansion into forests is predominantly distributed in Brazil in South America, the southern coast of West Africa, East Africa, and mainland Southeast Asia (Fig. 6a). Forest fires primarily occur in Siberia, Russia; Canada and Alaska in North America; the southern coast of Australia; and the southern edge of the Amazon in South America (Fig. 6b). Shifting agriculture is mainly concentrated in tropical regions, particularly in African forests, mainland and insular areas of Southeast Asia, and certain parts of Latin America (Fig. 6c). Global plantation-induced forest disturbances are primarily observed along the eastern coast of the United States, the southeastern coast of South America, Western Europe, Southeast Asia, and the southeastern coastal regions of China (Fig. 6d).



305

**Figure 6: Global Typical Forest Disturbance Statistics.** a. is the cropland occupation on forests; b. is the disturbance caused by forest fires; c. is the disturbance of shifting cultivation; d. is the disturbance of plantations (excluding oil palm).

Based on disturbance trajectories and recovery status, this study classified global forest cover into four categories: (a) disturbed then recovered, (b) disturbed but unrecovered, (c) undisturbed forests, and (d) newly established forests (Fig. 7).  
310 The recovered forests were predominantly located in wildfire-affected areas in North America and Siberia, plantation areas in Southeast Asia and the U.S. Eastern Seaboard, shifting cultivation regions across Southeast Asia, the Americas and Africa, as well as the Amazon rainforest (Fig. 7a). Unrecovered disturbed forests were primarily concentrated in cropland expansion areas of mainland Southeast Asia, South America and Africa (Fig. 7b). Globally undisturbed forests over the past two decades were mainly distributed across tropical rainforests in Africa, the Americas and Southeast Asia, along with primary  
315 forest regions in southeastern China, Russia, the United States and Canada (Fig. 7c). Newly added forest since the 2000 were principally found in India, China, southern Brazil, northern Australia, mountainous areas of the western United States, and Siberia (Fig. 7d).



320 **Figure 7 Global Forest Disturbance Characteristics.** a is recovered forest area; b is unrecovered disturbed area; c is undisturbed forest area; d is newly added forest area.

### 3.5 Spatial consistency with existing products

We compared the proportional characteristics of forest cover under the same drivers and disturbance types across different global regions. The accuracy of this study was determined by examining the spatial consistency between these two proportions. According to 200 grids covering a wide range of forest areas worldwide, the proportion of GFD in each grid has a high consistency with the proportion of CDGFL, with a consistency coefficient of 0.92 ( $R^2=0.93$ ). From the perspective of error, the MEA and RMSE of the two are only 13% and 19%, respectively (Fig. 8a). From the statistical proportion of different types of forest disturbance or forest loss drivers worldwide, both show forestry disturbance>shifting cultivation>forest fires>deforestation of natural forest. The spatial proportion of different forest disturbance types and forest loss driving types has a high consistency, with a consistency coefficient of 0.99 ( $R^2=0.99$ ) and an error of less than 5% (MAE=3.18%, RMSE=4.61%) (Fig. 8b).

325  
330

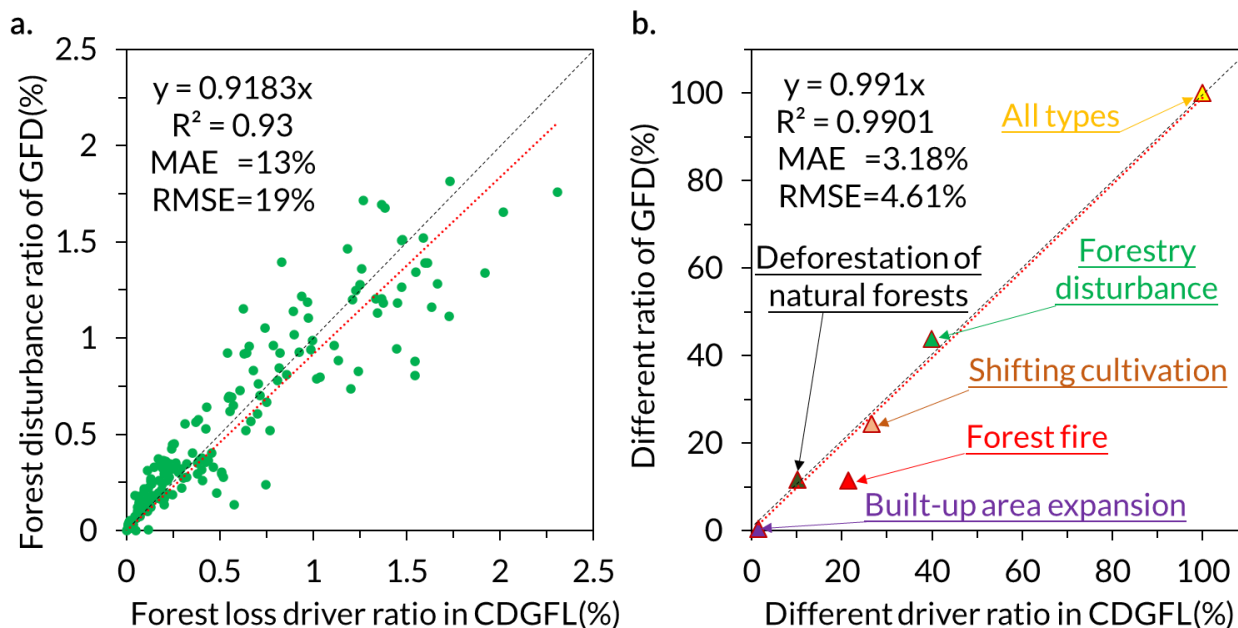


**Figure 8 Overall spatial consistency comparison with CDGFL.** a is the overall spatial consistency between the GFD mapping results and the CDGFL dataset. b is the consistency between different forest disturbance types of GFD and the CDGFL dataset.

Across different forest disturbance types, all categories exhibit strong spatial consistency with the existing CDGFL  
335 dataset (Fig. 9). We quantified the four dominant disturbance types with the largest proportions: forestry disturbance,  
shifting cultivation, forest fire, and deforestation of natural forests (Fig. 9). The comparative analysis reveals that these four  
major disturbance types display high spatial agreement with the existing low-resolution CDGFL dataset, with the following  
metrics: shifting cultivation ( $R^2=0.78$ , MEA=6.76%, RMSE=15.71%), forestry disturbance ( $R^2=0.83$ , MEA=10.61%,  
RMSE=17.49%), forest fire ( $R^2=0.85$ , MEA=5.93%, RMSE=12.17%), and deforestation of natural forest ( $R^2=0.62$ ,  
340 MEA=4.66%, RMSE=11.47%). Notably, forestry disturbance, despite having the highest consistency coefficient (0.91),  
shows the largest error index (RMSE=17.49%) (Fig. 9b). In contrast, deforestation of natural forest, with the lowest  
consistency coefficient (0.75), exhibits the smallest error index (RMSE=11.47%) (Fig. 9d). This discrepancy is likely  
attributable to the high degree of confusion between forestry disturbance and other disturbance types (Fig. 3). Furthermore,  
the substantial uncertainty ( $\pm 0.31\%$ ) in the area estimation of forestry disturbance further corroborates this observation  
345 (Table 5).

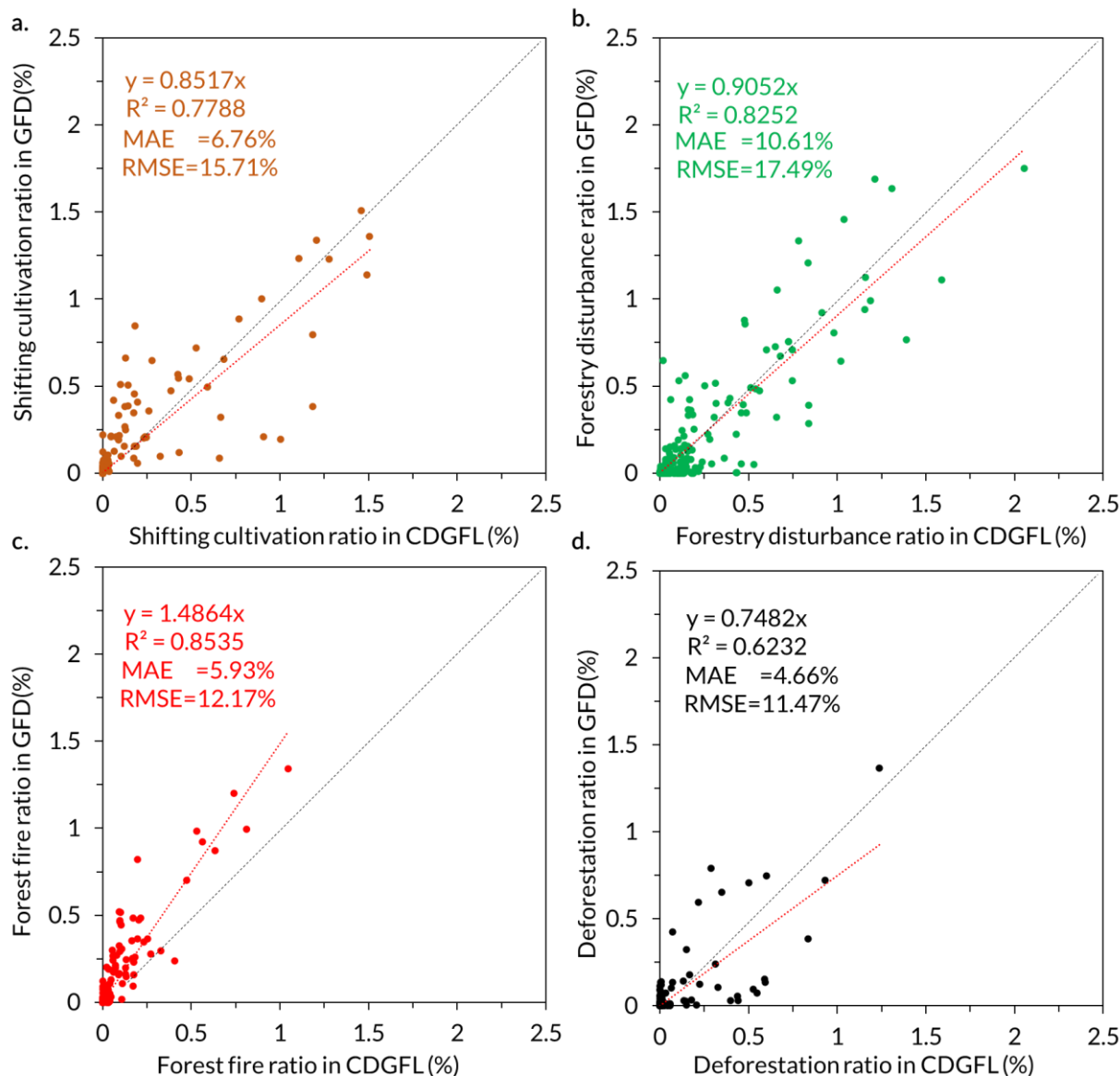


**Figure 9 Spatial consistency under different forest disturbance types.** a-d represent the spatial consistency of between the GFD and the CDGFL in shifting cultivation, forestry disturbance, forest fire, and deforestation of natural forest, respectively.

#### 4. Data availability

350 Landsat data and auxiliary data are sourced from public data archives and GEE's user team (<https://code.earthengine.google.com/> Last visit date: May 10, 2025). The GFD type map produced in this study is openly available at <https://doi.org/10.6084/m9.figshare.28465178> (Liu et al., 2025a).



## 5. Conclusion

The study presents the first high-resolution global forest disturbance (GFD) dataset, which significantly advances the monitoring and understanding of forest dynamics from 2000 to 2020. By integrating Landsat-based Continuous Change Detection and Classification (CCDC) time-series analysis with spatial predictors and machine learning techniques, the dataset achieves an impressive overall accuracy of 94.88%, demonstrating robust performance in classifying 11 major forest disturbance types. The results highlight forestry disturbance (43.79%), shifting cultivation (24.32%), and forest fires (11.45%) as the dominant drivers of global forest cover changes, collectively accounting for nearly 80% of the total disturbed area. These findings underscore the pervasive impact of anthropogenic activities and natural disturbances on forest ecosystems, with significant regional variations observed across tropical, temperate, and boreal forests.

The spatial distribution of disturbances reveals critical patterns: cropland expansion primarily affects forests in South America, West Africa, and Southeast Asia; forest fires are concentrated in Siberia, North America, and Australia; and shifting cultivation dominates tropical regions. The study also identifies areas of forest recovery, particularly in wildfire-affected zones and plantation regions, as well as newly established forests in countries like China, India, and Brazil. These insights are vital for informing targeted conservation strategies and climate change mitigation efforts, such as those under the Paris Agreement.

Despite its achievements, the study acknowledges limitations, including the exclusion of weak disturbances (drought and pests) due to data constraints and the challenges in distinguishing between certain disturbance types, such as forestry disturbance and deforestation. Future research should focus on incorporating higher-resolution data and refining classification algorithms to address these gaps. Nevertheless, the GFD dataset provides a valuable foundation for global forest governance, carbon accounting, and sustainable land management, offering policymakers and scientists a reliable tool to track forest changes and implement evidence-based interventions.

In conclusion, this study represents a significant step forward in global forest monitoring, combining advanced remote sensing technologies with machine learning to deliver a comprehensive, high-accuracy dataset. Its findings emphasize the urgent need for coordinated international efforts to mitigate forest degradation and promote restoration, ensuring the continued provision of essential ecosystem services in the face of escalating environmental challenges.

### Author contributions

SL and LW designed the research. LW, JZ, and SL performed the analysis. JZ, WS, SD, and LW collected the samples and existing remote sensing products. LW and SL wrote the manuscript. JZ, WS, and SD reviewed the manuscript.

### Competing interests

The contact author has declared that none of the authors has any competing interests.



## Acknowledgements

We thank the editor and the reviewers for their valuable comments.

## 385 Financial support

This work was supported by the National Key Research and Development Program of China (Grant No:2021YFE0117900), National Natural Science Foundation of China (Grant No: 42401082), Postdoctoral Fellowship Program of CPSF (Grant No: GZC20232757), and Project funded by China Postdoctoral Science Foundation (Grant No: 2024M763351).

## 390 References

- Acil, N., Sadler, J. P., Senf, C., Suvanto, S., and Pugh, T. A. M.: Landscape patterns in stand-replacing disturbances across the world's forests, *Nature Sustainability*, 8, 10.1038/s41893-024-01450-3, 2025.
- Aquino, C., Mitchard, E. T. A., McNicol, I. M., Carstairs, H., Burt, A., Vilca, B. L. P., Ebanega, M. O., Dikongo, A. M., Dassi, C., Mayta, S., Tamayo, M., Grijalba, P., Miranda, F., and Disney, M.: Reliably mapping low-intensity forest disturbance using satellite radar data, *Frontiers in Forests and Global Change*, 5, 10.3389/ffgc.2022.1018762, 2022.
- 395 Betts, M. G., Wolf, C., Ripple, W. J., Phalan, B., Millers, K. A., Duarte, A., Butchart, S. H. M., and Levi, T.: Global forest loss disproportionately erodes biodiversity in intact landscapes, *Nature*, 547, 441-+, 10.1038/nature23285, 2017.
- Blaschke, P. M., Trustrum, N. A., and Derose, R. C.: ECOSYSTEM PROCESSES AND SUSTAINABLE LAND-USE IN NEW-ZEALAND STEEPLANDS, *Agr. Ecosyst. Environ.*, 41, 153-178, 10.1016/0167-8809(92)90107-m, 1992.
- 400 Burrus, C. S., Barreto, J. A., and Selesnick, I. W.: ITERATIVE REWEIGHTED LEAST-SQUARES DESIGN OF FIR FILTERS, *Ieee Transactions on Signal Processing*, 42, 2926-2936, 10.1109/78.330353, 1994.
- Chen, S. J., Olofsson, P., Saphangthong, T., and Woodcock, C. E.: Monitoring shifting cultivation in Laos with Landsat time series, *Remote Sens. Environ.*, 288, 10.1016/j.rse.2023.113507, 2023a.
- Chen, X. L., Taylor, A. R., Reich, P. B., Hisano, M., Chen, H. Y. H., and Chang, S. X.: Tree diversity increases decadal forest soil carbon and nitrogen accrual, *Nature*, 618, 94-101, 10.1038/s41586-023-05941-9, 2023b.
- 405 Chowdhury, S., Chao, D. K., Shipman, T. C., and Wulder, M. A.: Utilization of Landsat data to quantify land-use and land-cover changes related to oil and gas activities in West-Central Alberta from 2005 to 2013, *Giscience & Remote Sensing*, 54, 700-720, 10.1080/15481603.2017.1317453, 2017.
- Cuni-Sanchez, A., Sullivan, M. J. P., Platts, P. J., Lewis, S. L., Marchant, R., Imani, G., Hubau, W., Abiem, I., Adhikari, H., Albrecht, T., Altman, J., Amani, C., Aneseyee, A. B., Avitabile, V., Banin, L., Batumike, R., Bauters, M., Beeckman, H., Begne, S. K., Bennett, A. C., Bitariho, R., Boeckx, P., Bogaert, J., Bräuning, A., Bulonvu, F., Burgess, N. D., Calders, K., Chapman, C., Chapman, H., Comiskey, J., de Haulleville, T., Decuyper, M., DeVries, B., Dolezal, J., Droissart, V., Ewango, C., Feyera, S., Gebrekirstos, A., Gereau, R., Gilpin, M., Hakizimana, D., Hall, J., Hamilton, A., Hardy, O., Hart, T., Heiskanen, J., Hemp, A., Herold, M., Hiltner, U., Horak, D., Kamdem, M. N., Kayijamahe, C., Kenfack, D.,



- 415 Kinyanjui, M. J., Klein, J., Lisingo, J., Lovett, J., Lung, M., Makana, J. R., Malhi, Y., Marshall, A., Martin, E. H.,  
Mitchard, E. T. A., Morel, A., Mukendi, J. T., Muller, T., Nchu, F., Nyirambangutse, B., Okello, J., Peh, K. S. H.,  
Pellikka, P., Phillips, O. L., Plumptre, A., Qie, L., Rovero, F., Sainge, M. N., Schmitt, C. B., Sedlacek, O., Ngute, A. S.  
K., Sheil, D., Sheleme, D., Simegn, T. Y., Simo-Droissart, M., Sonké, B., Soromessa, T., Sunderland, T., Svoboda, M.,  
Taedoumg, H., Taplin, J., Taylor, D., Thomas, S. C., Timberlake, J., Tuagben, D., Umunay, P., Uzabaho, E., Verbeeck,  
420 H., Vleminckx, J., Wallin, G., Wheeler, C., Willcock, S., Woods, J. T., and Zibera, E.: High aboveground carbon stock  
of African tropical montane forests, *Nature*, 596, 536–+, 10.1038/s41586-021-03728-4, 2021.
- Curtis, P. G., Slay, C. M., Harris, N. L., Tyukavina, A., and Hansen, M. C.: Classifying drivers of global forest loss, *Science*,  
361, 1108–1111, 10.1126/science.aau3445, 2018.
- Feng, Y., Ziegler, A. D., Elsen, P. R., Liu, Y., He, X. Y., Spracklen, D. V., Holden, J., Jiang, X., Zheng, C. M., and Zeng, Z.  
425 Z.: Upward expansion and acceleration of forest clearance in the mountains of Southeast Asia, *Nature Sustainability*, 4,  
892–899, 10.1038/s41893-021-00738-y, 2021.
- Finger, D. J. I., McPherson, M. L., Houskeeper, H. F., and Kudela, R. M.: Mapping bull kelp canopy in northern California  
using Landsat to enable long-term monitoring, *Remote Sens. Environ.*, 254, 10.1016/j.rse.2020.112243, 2021.
- Hansen, M. C., Potapov, P. V., Moore, R., Hancher, M., Turubanova, S. A., Tyukavina, A., Thau, D., Stehman, S. V., Goetz,  
430 S. J., Loveland, T. R., Kommareddy, A., Egorov, A., Chini, L., Justice, C. O., and Townshend, J. R. G.: High-Resolution  
Global Maps of 21st-Century Forest Cover Change, *Science*, 342, 850–853, 10.1126/science.1244693, 2013.
- Hwang, Y., Ryu, Y., and Qu, S.: Expanding vegetated areas by human activities and strengthening vegetation growth  
concurrently explain the greening of Seoul, *Landscape Urban Plann.*, 227, 10.1016/j.landurbplan.2022.104518, 2022.
- Jiang, S., Meng, J. J., Zhu, L. K., and Cheng, H. R.: Spatial-temporal pattern of land use conflict in China and its multilevel  
435 driving mechanisms, *Sci. Tot. Environ.*, 801, 10.1016/j.scitotenv.2021.149697, 2021.
- Kittel, T. G. F., Steffen, W. L., and Chapin, F. S.: Global and regional modelling of Arctic-boreal vegetation distribution and  
its sensitivity to altered forcing, *Global. Change. Biol.*, 6, 1–18, 10.1046/j.1365-2486.2000.06011.x, 2000.
- Leverkus, A. B., Lindenmayer, D. B., Thorn, S., and Gustafsson, L.: Salvage logging in the world's forests: Interactions  
440 between natural disturbance and logging need recognition, *Global Ecol. Biogeogr.*, 27, 1140–1154, 10.1111/geb.12772,  
2018.
- Liu, S., Wang, L., and Song, W.: Global forest main disturbance types between 2000 and 2020,  
10.6084/m9.figshare.28465178.v1, 2025a.
- Liu, S., Wang, L., and Zhang, J.: The dataset of main grain land changes in China over 1985–2020, *Scientific Data*, 11, 1430,  
10.1038/s41597-024-04292-y, 2024.
- 445 Liu, S., Wang, L., Zhang, J., and Ding, S.: Opposite effect on soil organic carbon between grain and non-grain crops:  
Evidence from Main Grain Land, China, *Agric., Ecosyst. Environ.*, 379, 109364,  
<https://doi.org/10.1016/j.agee.2024.109364>, 2025b.
- Mason, K. E., Oakley, S., Street, L. E., Arróniz-Crespo, M., Jones, D. L., DeLuca, T. H., and Ostle, N. J.: Boreal Forest Floor



- Greenhouse Gas Emissions Across a Pleurozium schreberi-Dominated, Wildfire-Disturbed Chronosequence, *Ecosystems*, 22, 1381-1392, 10.1007/s10021-019-00344-2, 2019.
- 450 Mayer, M., Baltensweiler, A., James, J., Rigling, A., and Hagedorn, F.: A global synthesis and conceptualization of the magnitude and duration of soil carbon losses in response to forest disturbances, *Global Ecol. Biogeogr.*, 33, 141-150, 10.1111/geb.13779, 2024.
- Miatto, A., Dawson, D., Nguyen, P. D., Kanaoka, K. S., and Tanikawa, H.: The urbanisation-environment conflict: Insights  
455 from material stock and productivity of transport infrastructure in Hanoi, Vietnam, *J. Environ. Manage.*, 294, 10.1016/j.jenvman.2021.113007, 2021.
- Oeser, J., Heurich, M., Senf, C., Pflugmacher, D., and Kuemmerle, T.: Satellite-based habitat monitoring reveals long-term dynamics of deer habitat in response to forest disturbances, *Ecol. Appl.*, 31, 10.1002/eap.2269, 2021.
- Olofsson, P., Foody, G. M., Herold, M., Stehman, S. V., Woodcock, C. E., and Wulder, M. A.: Good practices for estimating  
460 area and assessing accuracy of land change, *Remote Sens. Environ.*, 148, 42-57, 10.1016/j.rse.2014.02.015, 2014.
- Peng, L. Q., Searchinger, T. D., Zions, J., and Waite, R.: The carbon costs of global wood harvests, *Nature*, 620, 110-+, 10.1038/s41586-023-06187-1, 2023.
- Piao, S. L., Wang, X. H., Park, T., Chen, C., Lian, X., He, Y., Bjerke, J. W., Chen, A. P., Ciais, P., Tommervik, H., Nemani, R.  
465 R., and Myneni, R. B.: Characteristics, drivers and feedbacks of global greening, *Nature Reviews Earth & Environment*, 1, 14-27, 10.1038/s43017-019-0001-x, 2020.
- Reza, M. I. H. and Abdullah, S. A.: Regional Index of Ecological Integrity: A need for sustainable management of natural resources, *Ecol. Indicators*, 11, 220-229, 10.1016/j.ecolind.2010.08.010, 2011.
- Rivera, J. D., de los Monteros, A. E., Saldaña-Vázquez, R. A., and Favila, M. E.: Beyond species loss: How anthropogenic disturbances drive functional and phylogenetic homogenization of Neotropical dung beetles, *Sci. Tot. Environ.*, 869,  
470 10.1016/j.scitotenv.2023.161663, 2023.
- Roffe, T. G., Couturier, S., and García-Romero, A.: Suitability of the global forest cover change map to assess climatic megadisturbance impacts on remote tropical forests, *Sci. Rep.*, 12, 10.1038/s41598-022-13558-7, 2022.
- Ross, M. R. V., Nippgen, F., McGlynn, B. L., Thomas, C. J., Brooks, A. C., Shriver, R. K., Moore, E. M., and Bernhardt, E.  
475 S.: Mountaintop mining legacies constrain ecological, hydrological and biogeochemical recovery trajectories, *Environ. Res. Lett.*, 16, 10.1088/1748-9326/ac09ac, 2021.
- Scheeres, J., de Jong, J., Brede, B., Brancalion, P. H. S., Broadbent, E. N., Zambrano, A. M. A., Gorgens, E. B., Silva, C. A.,  
Valbuena, R., Molin, P., Stark, S., Rodrigues, R. R., Rodrigues, R., Santoro, G. B., de Almeida, C. T., and de Almeida,  
D. R. A.: Distinguishing forest types in restored tropical landscapes with UAV-borne LIDAR, *Remote Sens. Environ.*,  
290, 10.1016/j.rse.2023.113533, 2023.
- 480 Scholten, R. C., Jandt, R., Miller, E. A., Rogers, B. M., and Veraverbeke, S.: Overwintering fires in boreal forests, *Nature*, 593, 399-+, 10.1038/s41586-021-03437-y, 2021.
- Skakun, S., Vermote, E. F., Artigas, A. E. S., Rountree, W. H., and Roger, J. C.: An experimental sky-image-derived cloud



- validation dataset for Sentinel-2 and Landsat 8 satellites over NASA GSFC, *Int. J. Appl. Earth Obs. Geoinf.*, 95, 10.1016/j.jag.2020.102253, 2021.
- 485 Skidmore, A. K., Coops, N. C., Neinavaz, E., Ali, A., Schaepman, M. E., Paganini, M., Kissling, W. D., Vihervaara, P., Darvishzadeh, R., Feilhauer, H., Fernandez, M., Fernández, N., Gorelick, N., Geizendorffer, I., Heiden, U., Heurich, M., Hobern, D., Holzwarth, S., Muller-Karger, F. E., Van De Kerchove, R., Lausch, A., Leitau, P. J., Lock, M. C., Mücher, C. A., O'Connor, B., Rocchini, D., Turner, W., Vis, J. K., Wang, T. J., Wegmann, M., and Wingate, V.: Priority list of biodiversity metrics to observe from space, *Nature Ecology & Evolution*, 5, 896-906, 10.1038/s41559-021-01451-x, 490 2021.
- Tollerud, H. J., Zhu, Z., Smith, K., Wellington, D. F., Hussain, R. A., and Viola, D.: Toward consistent change detection across irregular remote sensing time series observations, *Remote Sens. Environ.*, 285, 10.1016/j.rse.2022.113372, 2023.
- Tong, X. W., Brandt, M., Yue, Y. M., Ciais, P., Jepsen, M. R., Penuelas, J., Wigneron, J. P., Xiao, X. M., Song, X. P., Horion, S., Rasmussen, K., Saatchi, S., Fan, L., Wang, K. L., Zhang, B., Chen, Z. C., Wang, Y. H., Li, X. J., and Fensholt, R.: 495 Forest management in southern China generates short term extensive carbon sequestration, *Nat. Commun.*, 11, 10.1038/s41467-019-13798-8, 2020.
- Wang, D. C., Chen, X. N., Jiang, M. Y., Du, S. H., Xu, B. J., and Wang, J. D.: ADS-Net: An Attention-Based deeply supervised network for remote sensing image change detection, *Int. J. Appl. Earth Obs. Geoinf.*, 101, 10.1016/j.jag.2021.102348, 2021.
- 500 Xu, R., Li, Y., Teuling, A. J., Zhao, L., Spracklen, D., Garcia-Carreras, L., Meier, R., Chen, L., Zheng, Y. T., Lin, H. Q., and Fu, B. J.: Contrasting impacts of forests on cloud cover based on satellite observations, *Nat. Commun.*, 13, 10.1038/s41467-022-28161-7, 2022.
- Yan, X. R., Wang, J. L., Liu, X. T., Zhao, H. Y., and Wu, Y. X.: Mining the drivers of forest cover change in the upper Indus Valley, high Asia region from 1990 to 2020, *Ecol. Indicators*, 144, 10.1016/j.ecolind.2022.109566, 2022.
- 505 Yang, Y., Anderson, M., Gao, F., Hain, C., Noormets, A., Sun, G., Wynne, R., Thomas, V., and Sun, L.: Investigating impacts of drought and disturbance on evapotranspiration over a forested landscape in North Carolina, USA using high spatiotemporal resolution remotely sensed data, *Remote Sens. Environ.*, 238, 10.1016/j.rse.2018.12.017, 2020.
- Ygorra, B., Frappart, F., Wigneron, J. P., Moisy, C., Catry, T., Baup, F., Hamunyela, E., and Riazanoff, S.: Monitoring loss of tropical forest cover from Sentinel-1 time-series: A CuSum-based approach, *Int. J. Appl. Earth Obs. Geoinf.*, 103, 510 10.1016/j.jag.2021.102532, 2021.
- Zhao, Y. L., Diao, C. Y., Augspurger, C. K., and Yang, Z. J.: Monitoring spring leaf phenology of individual trees in a temperate forest fragment with multi-scale satellite time series, *Remote Sens. Environ.*, 297, 10.1016/j.rse.2023.113790, 2023.
- Zhu, Z. and Woodcock, C. E.: Continuous change detection and classification of land cover using all available Landsat data, 515 *Remote Sens. Environ.*, 144, 152-171, 10.1016/j.rse.2014.01.011, 2014.